Effect of Random End-Linking on the Viscoelastic Relaxation of Entangled Star Polymers

Erwan Nicol, Taco Nicolai,* and Dominique Durand

Polymères, Colloïdes, Interfaces, UMR CNRS 6120, Université du Maine, 72085 Le Mans Cedex 9, France

Received December 27, 2000; Revised Manuscript Received May 9, 2001

ABSTRACT: Dynamic mechanical measurements are presented for poly(propylene) sulfide (PPS) stars with a range of molar masses. The results are shown to be consistent with theoretical predictions. The effect of end-linking on the viscoelastic relaxation of entangled stars is studied at various connectivity extents. We show that scaling theories are not suited to describe the relaxation of end-linked entangled stars in the frequency range that is experimentally accessible.

Introduction

A large class of polymeric gels, such as natural rubbers, are formed by cross-linking entangled polymers in the melt. Increasing the connectivity extent (p) leads to the formation of larger branched polymers until at a critical value (p_c) a gel is formed. The approach of the gel point is characterized by a diverging viscosity for $p_- \rightarrow p_c$ and a disappearing gel modulus for $p_+ \rightarrow p_c$. At the gel point the loss and storage shear modulus have a power law frequency dependence at low frequencies with the same exponent.

The viscoelastic relaxation of polymeric gels close to the gel point has received much attention.[1−18] For many systems the results turn out to be consistent with the percolation model,[1−10] but different behavior has also been reported.[10−18] On the other hand, exploration of the viscoelastic properties of cross-linked systems from the precursor polymers to the fully cross-linked gel and covering the full dynamical range is rare. Full exploration is not only more useful from a practical point of view, but it also makes more apparent the range of cross-link densities and frequencies where the system shows the critical behavior of the sol−gel transition.

In earlier work we have reported such an investigation for unentangled poly(propylene oxide) (PPO) stars end-linked by diisocyanate.[19] The results show that the viscoelastic relaxation at low frequencies is compatible with the percolation model very close to the gel point but that it is important to consider the finite size of the branched polymers. Above the gel point we observed slow relaxation processes on length scales much larger than the average distance between cross-links. The slow relaxation is seen even for highly cross-linked gels and points to restructuring of the gel on large length scales in response to a deformation.

In the description of the viscoelastic relaxation using the percolation model, it has been assumed that the polymers are not entangled. This assumption is reasonable if the precursors are smaller than the length needed to form entanglements. For such systems the distance between branch points is smaller than the entanglement length. The size distribution and the structure of the branched polymers are such that polymers of the same size do not strongly overlap, but small polymers penetrate the larger polymers. The situation is very different if the precursors are already strongly entangled. The effect of entanglements on the viscoelastic relaxation of randomly branched polymers is still largely unexplored and is the topic of this paper.

In the next section we will summarize the theoretical background used for the interpretation of the results. Then we will show that the viscoelastic relaxation of poly(propylene sulfide) (PPS) stars with a range of molar masses (0.8−60 kg/mol) is well-described by the theory. Finally, we will present and discuss the viscoelastic relaxation of end-linked entangled PPS stars with different degrees of end-linking.

Theoretical Background

The viscoelastic relaxation of entangled linear flexible polymers in response to mechanical deformation is an old problem and has been extensively studied.[20] At a given temperature the response is solidlike at high frequencies, but often some relaxation occurs due to localized motion. At lower frequencies the system relaxes due to cooperative motion of the chain backbone segments: the so-called α-relaxation. The lower the frequency, the larger the size of the chain backbone that can relax its conformation in response to the deformation. The conformational relaxation on large length scales is hindered by topological constraints caused by other chains, and they have to disentangle from each other before the system can relax fully. It turns out that the effect of topological constraints can be modeled by assuming that they form a tube around the chains which limits the lateral motion.[21] The diameter of the tube is equal to the average distance between entanglements (ξ_e). On length scales smaller than ξ_e the conformational relaxation is well-described in terms of a series of normal modes with screened hydrodynamic interactions (Rouse modes). Larger scale conformational relaxation is due to a snakelike motion (reptation) through the tube, which relaxes the conformation first at the chain ends and progressively further along the chain backbone. The system has relaxed fully if the chains have diffused over the whole length of the tube, which is proportional to the chain length.

More recently, polymers with more complex architectures have been considered such as star- and H-shaped polymers.[22] Conformational relaxation on length scales smaller than ξ_e, i.e., inside the tube, can still be described in terms of Rouse modes, but obviously reptation is no longer possible if the polymers are branched. Conformational relation on larger length

10.1021/ma002202l CCC: $20.00
Published on Web 06/19/2001

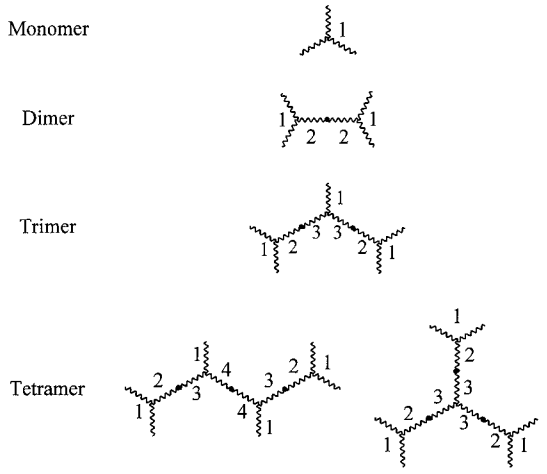

Figure 1. Schematic drawing of the first four oligomers of end-linked PPS stars. The numbers indicate the seniority of the arms.

scales occurs by the much slower process of arm retraction inside its tube and is only completed if the arm retraction has proceeded all the way to the branch point. If the polymers contain more than one branch point, the inner segments can only relax their conformation if the branch points closer to the chain ends have relaxed.

The tube model has been successful in describing the viscoelastic relaxation of systems with well-defined structures, after it was realized that the topological constraints that make up the tube around a particular chain are not permanent but disappear progressively due to reptation or arm retraction of the other chains.[22] This process is called dynamic dilution because with time more and more chain segments relax and dilute the remaining chain fragments that have not yet relaxed. Dynamic dilution reduces the density of constraints and thus speeds up the conformational relaxation.

However, the calculations become rapidly unwieldy if the complexity of the architecture of the polymers and the number of components are increased. Therefore, explicit calculation of the conformational relaxation of polydisperse randomly branched entangled polymers is not feasible, and a different approach is needed. Rubinstein et al.[23] have addressed the relaxation of large randomly branched polymers formed by end-linking linear chains with a multifunctional linking agent. They used mean field theory to calculate the average structure and the size distribution of the branched polymers. Here we apply their approach to the system used in the present study, i.e., randomly branched polymers formed by end-linking three-armed stars with a bifunctional linking agent.

The branched polymers may be visualized as treelike structures because the use of mean field theory implies that they do not contain loops. Clearly, a given segment of the branched polymer can only relax if all the other segments connected to it either to one side or to the other have relaxed. Conformational relaxation starts at the edges and progresses inward. To quantify this hierarchical relaxation process, Rubinstein et al. introduced the concept of seniority of chain segments between branch points. This chain segment is the trunk of two trees for which the largest chemical path to the edge contains s_1 and s_2 segments, respectively. The seniority of the segment is defined as $s = \min(s_1, s_2)$; see Figure 1.

A given segment will begin to relax its conformation once the shortest tree to which it is connected has fully relaxed. Thus, the time scale for the relaxation of segment with seniority s is set by the relaxation time of segments with seniority $s - 1$. The relaxation time of a segment with seniority $s > 1$ is given by

$$\tau(s) \approx \tau(s-1)\left(\frac{M}{M_e(s)}\right)^{0.5} \exp\left(\frac{\nu M}{M_e(s)}\right) \quad M > M_e(s) \quad (1)$$

where M is the molar mass of the segment which is in our case an arm of the PPS star. The tube model gives $\nu = 15/8$, but the effect of dynamic dilution during the relaxation of a given segment reduces this value somewhat. $M_e(s)$ is the effective entanglement molar mass at the time scale when the relaxation of segments with seniority s takes place. Dynamic dilution means that $M_e(s)$ depends on the volume fraction of segments that have not yet relaxed, i.e., with seniority s or larger ($\Phi(s)$):

$$M_e(s) = \frac{M_e}{\Phi(s)^\alpha} \quad (2)$$

where M_e is the entanglement molar mass of an arm in the melt. Rubinstein et al. used $\alpha = 1$, but it has been argued that one should use $\alpha = {}^4/_3$.[24,25] $\Phi(s) = \sum_{s'>s}^{\infty}\phi(s')$, with $\phi(s)$ the volume fraction of segments with seniority s. $\Phi(s)$ is unity for $s = 1$ and decreases with increasing s. This means that $M_e(s)$ increases with s and becomes larger than M at some value $s = s^*$. The relaxation process of segments with seniority $s \geq s^*$ is the same as for unentangled branched polymers and may be described in terms of Rouse modes. The prefactor which sets the time scale for these slow Rouse modes is $\tau(s^*)$.

For times between $\tau(1)$ and $\tau(s^*)$ the relaxation of the shear modulus is given by

$$G(t) = G(0)\left[\sum_{s=1}^{\infty}\phi(s)\exp(-t/\tau(s))\right]^{1+\alpha} \qquad \tau(s^*) > t > \tau(1) \quad (3)$$

At shorter times $G(t)$ is similar to that of the precursor stars, while at longer times the decay of $G(t)$ is due to the relaxation of effectively unentangled arms. For $t \gg \tau(1)$ the exponential may be approximated by a step function so that the relaxation spectrum of the shear modulus for intermediate times is easily calculated once we know $\phi(s)$.

To calculate $\phi(s)$, we need the probability, $P(n)$, that the longest chemical path of the tree connected to a segment in one given direction contains n segments. In mean field theory it is assumed that the probability of end-linking is independent of the position of the chain ends and that there is no cyclization. With these assumptions $P(n)$ is obtained by iteration as a function of the fraction of end-linked arms (p):

$$P(n) = P(n-1)\left[\sum_{i=1}^{n-2}2P(i) + P(n-1)\right] \quad n = 4, 6, 8, \ldots$$

$$P(n) = rP(n-1) \quad n = 3, 5, 7, \ldots \quad (4)$$

with

$$P(1) = (1 - r) \qquad P(2) = (1 - r)^2$$

The difference between odd and even values of n can be understood as follows: Segments with odd n are connected via a urethane link to segments with $n - 1$, except for $n = 1$ when it is a free end (see Figure 1). The probability that the link is formed is simply r. On the other hand, segments with even n are connected to two segments that belong to the same triol. We are interested in the longest chemical path so one segment is at $n - 1$ and the other segment is either at $n - 1$ or smaller values. The factor of 2 comes from the fact that we can choose either one of the segments to be at $n - 1$. The seniority of a segment is n unless the tree connected to this segment in the other direction is shorter. The fraction of segments with seniority s is thus given by

$$\phi(s) = P(s)\left[1 - r\sum_{i=1}^{s/2} P(2i - 1)\right] \quad n = 4, 6, 8, \ldots$$

$$\phi(s) = P(s)\left[1 - r\sum_{i=1}^{(s-1)/2} P(2i)\right] \quad n = 3, 5, 7, \ldots \quad (5)$$

with

$$\phi(1) = P(1) \qquad \phi(2) = rP(2)$$

In Figure 2 we have plotted $\phi(s)$ and $\Phi(s)$ for various values of $p < p_c = 0.5$. The strong decreases of $\Phi(s)$ with increasing s shows that dynamic dilution is very effective in releasing the topological constraints for segments with higher seniority. For s larger than $s_{min} \approx 50$, both $\phi(s)$ and $\Phi(s)$ have a power law dependence which is cut off by an exponential at s_{max}: $\phi(s) \propto s^{-3}$ and $\Phi(s) \propto s^{-2}$. The exponents of the power law relations do not depend on the functionality of the linking agent. Rubinstein et al. used these power law relations to derive an approximate analytical expression for $G(t)$ in the range $\min(\tau(s_{max}), \tau(s^*)) > t > \tau(s_{min})$. Figure 2 shows that s_{max} increases with the amount of end-linking and diverges at p_c, but s_{max} is larger than s_{min} only very close to the gel point. We have calculated s^* as a function of M_e/M using eq 2 and setting $M_e(s^*) = M$:

$$\Phi(s^*)^{-\alpha} = M_e/M \quad (6)$$

The results are plotted for different values of p in Figure 3 using $\alpha = {}^4/_3$. The decay of $G(t)$ derived by Rubinstein et al. may in theory be observed if both s_{max} and s^* are larger than s_{min}, i.e., very close to the gel point using precursors with $M/M_e > 1000$. But in practice it is not accessible experimentally, because for $M/M_e > 1000$ even the terminal relaxation of a free end is already far too slow (see below). The conclusion is essentially the same if we assume that $\alpha = 1$.

Experimental Section

Synthesis and Characterization of PPS Stars. We have synthesized a series of three-armed star PPS samples with −SH end groups following a procedure detailed in ref 26. A coupling reaction occurs at the end of the reaction due to the presence of trace oxygen, which leads to the formation of a small fraction of end-linked stars which are mainly dimers.

The samples were characterized using size exclusion chromatography (SEC) in the same way as reported earlier for linear PPS.[27] The chromatograms are very similar to those of linear PPS and show narrow peaks corresponding to the PPS stars and a small second peak corresponding to the dimers

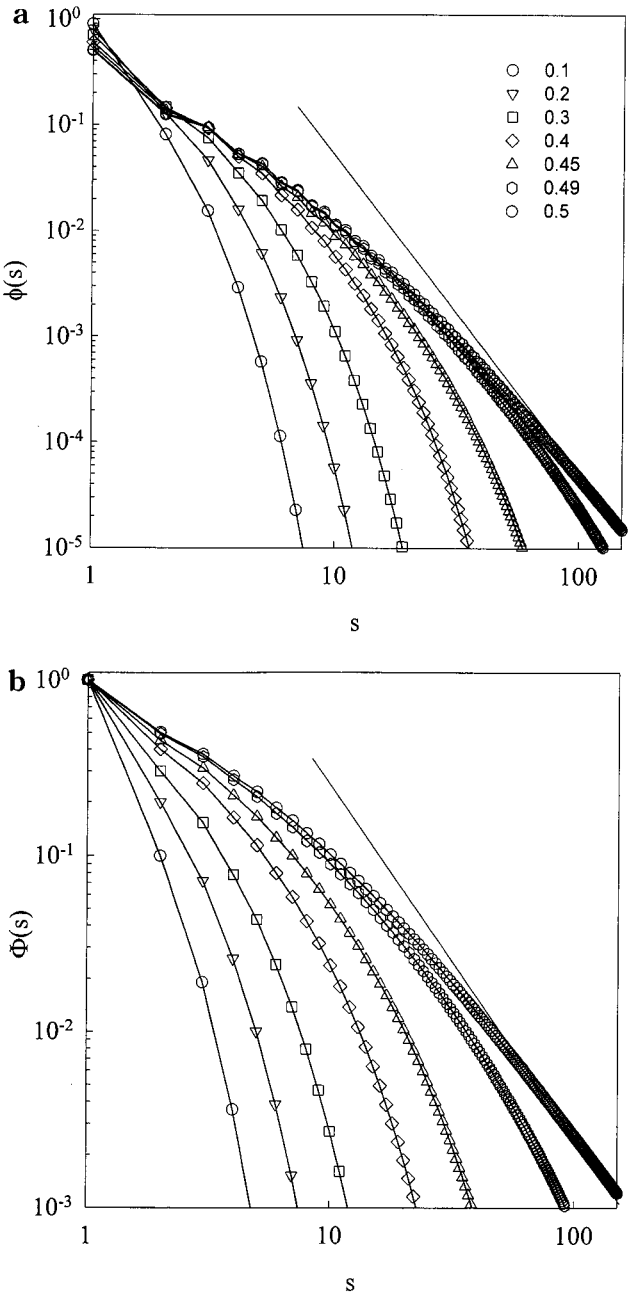

Figure 2. (a) Double-logarithmic representation of the fraction of star arms as a function of their seniority at different connectivity extents. The straight line has slope −2. (b) Double-logarithmic representation of the fraction of star arms with seniority larger than or equal to s ($\Phi(s) = \sum_{s'>s}^{\infty}\phi(s')$) as a function of s at different connectivity extents. The straight line has slope −3. Symbols are as in (a).

with twice the molar mass. We calculated the number (M_n) and weight (M_w) averaged molar masses of the stars using the calibration curve of polystyrene standards. The absolute value of M_w was determined for the three largest samples in dilute solution in THF using light scattering. The scattering by the smaller samples is too weak to obtain accurate results. For two smaller samples the molar mass was determined with mass spectroscopy (MALDI-TOF). The results are summarized in Table 1 and are for most samples close to the values aimed for in the synthesis. Within the experimental error the molar mass obtained from light scattering or mass spectroscopy happens to be the same as the equivalent molar mass of polystyrene obtained from SEC. The increase of the polydispersity index ($I_p = M_n/M_w$) with the size of the PPS stars is caused by the increasing amount of coupling. The polydispersity index of just the stars is about 1.04 independent of their

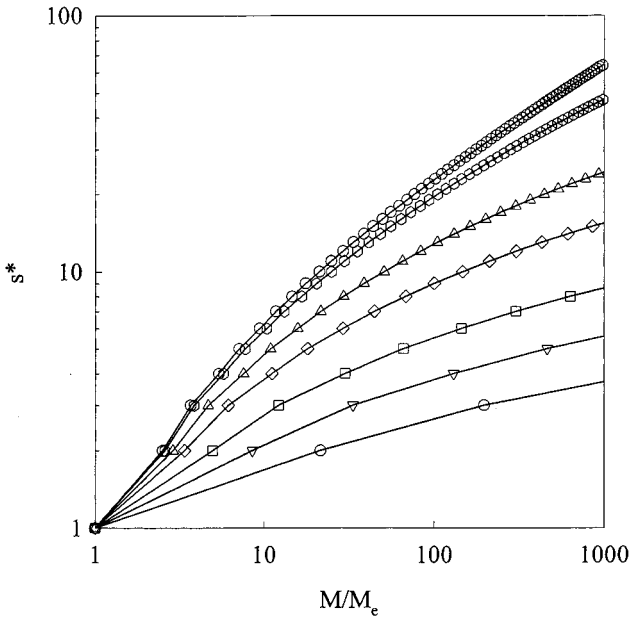

Figure 3. Double-logarithmic representation of the maximum seniority of arms that are still effectively entangled when they relax their conformation, as a function of the number of entanglements of the precursors. Symbols as in Figure 2a.

size. The number of segments per arm (n_a) was calculated using M_n obtained from SEC after correcting for the fraction of dimers.

The calorimetric glass transition temperatures were measured with an accuracy of ±2 deg using differential scanning calorimetry. The samples were rapidly cooled to 150 K and then heated at a rate of 10 K/min. Values of T_g are summarized in Table 1 and plotted in Figure 4 as a function $1/n_a$. For comparison, we included the results reported earlier for linear PPS which may be considered as two-armed stars.[27] The linear least-squares fit gives for star PPS

$$T_g = 236.8 - \frac{73}{n_a}\,(\mathrm{K}) \tag{7a}$$

and for linear PPS

$$T_g = 237.2 - \frac{125}{n_a}\,(\mathrm{K}) \tag{7b}$$

The decreases of T_g with decreasing n_a due to the effect of free ends is less important for star PPS, which contains a core that rigidifies the structure and compensates partially for the effect of free ends. For large n_a both the core and free end effects become negligible so that linear and star PPS have the same glass transition temperature.

Synthesis and Characterization of End-Linked PPS Stars. PPS stars with $n_a = 72$ (T5) were end-linked by hexamethyl diisocyanate (HMDI) in the presence of a small amount of catalyst (dibutyl tin dilaurate). The ingredients were thoroughly mixed at room temperature, after which the reaction was left to complete by keeping the sample at 60 °C for at least 15 h. Samples were prepared at different stoichiometric ratios of isocyanate and thiol groups r = [NCO]/[SH]. PPS stars with $n_a = 263$ (T7) were end-linked in the reaction bath by addition of different amounts of hydrogen peroxide at the end of the polymerization. This means that for this sample end-linking did not take place in the melt but at a volume fraction of about 25%. End-linked T7 samples were precipitated, and the residual solvent was removed under vacuum in the same way as for the precursors.

The end-linked samples were characterized with SEC following a method used earlier to characterize end-linked PPO stars.[28] Chromatograms of end-linked samples are shown in Figure 5. One can distinguish monomers, dimers, and trimers, but larger particles are eluted as a continuous distribution. A small peak is visible at larger retention volumes than the monomer, which corresponds to a very small fraction (<5%) of monofunctional single arms. We have determined the fractions of monomers, dimers, and trimers for each sample, and we have compared the results with the mean field prediction. We deduced the fraction of end-linked arms p, i.e., the connectivity extent, by taking those values that give best agreement for all three fractions (see Figure 6). The values of p are summarized in Table 2 together with M_w and I_p obtained from SEC. We verified for a few samples that M_w obtained from SEC is close to that obtained with light scattering. The dependence of M_w and I_p on p agrees with the mean field prediction; see ref 28 where we discussed this point for the case of PPO stars. As mentioned above, a trace amount of oxygen in the reaction bath causes some end-linking and explains why p is not zero in the absence of added linking agent.

In the ideal case p is equal to r and $r_c = 0.5$ according to mean field theory. However, even for small PPO stars end-linked with HDMI we observed that r_c was significantly larger than 0.5, and the deviation increased with increasing n_a (r_c = 0.52−0.8 for $n_a = 1-45$).[29] T5 with $n_a = 72$ formed a gel at $r = 1$ but did not gel for $r \leq 0.8$. Several reasons may be invoked to explain a larger value of r_c: impurity of the diisocyanate, formation of cycles, incomplete reaction, and side reactions. The dominant contribution to the large deviation of r_c from 0.5 for T5 is most likely the side reactions of isocyanate, which become more probable with decreasing density of SH groups and increasing viscosity of the system.

End-linking PPS with HMDI leads to an increase of the glass transition temperature due to the formation of thiolcarbamate links,[30] but the effect on T_g is negligible for the large precursors used in this study.

Dynamic Mechanical Measurements. Dynamic shear measurements were made on a Rheometrics RDA II dynamic spectrometer using parallel-plate geometry at temperatures between 200 and 340 K. The so-called hold mode was used where the gap is corrected for temperature variations of the sample volume. The plate size (diameters 25, 8, and 4 mm) and the imposed deformation (0.1−100%) were adjusted to obtain an accurate torque response while remaining in the linear regime. The shear modulus could be measured in the range $10-10^9$ Pa. We were able to measure very large moduli by using a relatively large sample thickness (2−2.5 mm) in combination with a small plate size. The range of radial frequencies, ω, used was 0.01−100 rad/s. Temperatures were measured using a thermocouple close to the lower plate. The temperature was stable within ±0.2 K over the whole range used in this study (200−350 K).

Results and Discussion

Viscoelastic Relaxation of PPS Stars. The storage ($G'(\omega)$) and loss ($G''(\omega)$) shear moduli were measured between 0.01 and 100 rad/s over a wide range of temperatures. When we attempted to superimpose the data obtained at different temperatures, we noticed that the temperature dependence of the α-relaxation is slightly stronger than that of the slower conformational relaxation. A different temperature dependence has been observed for many systems.[31] The difference is the same for all systems studied here and is identical to that of PPO for which it was studied in detail.[32] Master curves could nevertheless be obtained by choosing a reference temperature (T_{ref}) such that both types of relaxation are clearly visible. We superimposed the high-frequency data of measurements done at $T < T_{ref}$ and the low-frequency data of measurements done at $T > T_{ref}$. Details of this procedure may be found in ref 32. The resulting master curve is characteristic for the system at $T = T_{ref}$ and looks slightly different for other reference temperatures. Master curves for different

Table 1. Characteristics of PPS Star Polymers

	M_w (kg/mol) (SEC)[a]	M (kg/mol)	n_a	M_w/M_n	coupling (%)	T_g (K)	T_{gv} (K)	$\log(\tau_a/s)$
T1	0.8	0.83[b]	3	1.04	2	215	210	−10.5
T2	1.5		6	1.05	5	226	220	−10.1
T3	2.7	3.05[b]	11	1.09	8	230	226	−9.8
T4	4.6		18	1.09	10	233	228	−9.3
T5	18.9	18.7[c]	72	1.13	13	236	230	−8.0
T6	35.5	29.2[c]	128	1.12	12	236	231	−7.3
T7	71.2	68.5[c]	263	1.18	17	236.5	232	−6.1

[a] Using calibration with polystyrene standards. [b] The major peak observed in MALDI-TOF mass spectroscopy. [c] M_w obtained from light scattering.

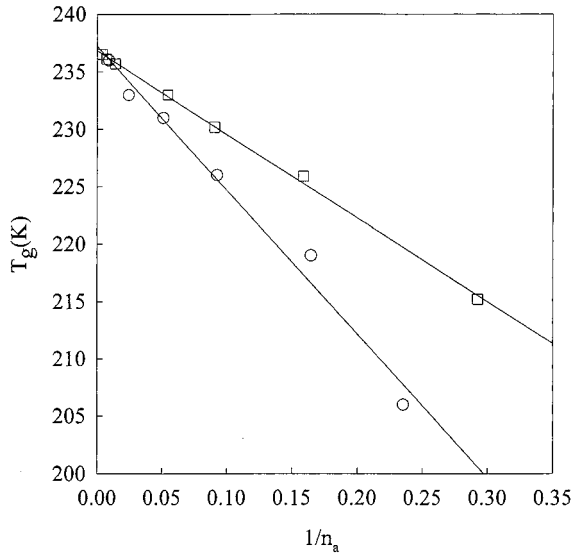

Figure 4. Dependence of the glass transition temperature of linear (circles) and star (squares) PPS on the inverse number of segments per arm. Linear PPS is considered as a star with two arms. The straight lines represent linear least-squares fits; see eq 7.

systems are comparable if we chose T_{ref} at the same distance from the glass transition temperature.

Figure 7 shows master curves of the storage and loss shear modulus of PPS stars with n_a ranging between 3 and 263. The α-relaxation at high frequencies crosses over to the conformational relaxation that extends to lower frequencies as the molar mass is increased. For all master curves we have used $T_{ref} = T_{gv} + 5$ K, where T_{gv} is defined as the temperature where the loss peak of the α-relaxation is situated at $\omega_{max} = 1$ rad/s. T_{gv} is systematically about 5 deg lower than the calorimetric glass transition temperature (see Table 1). As was discussed in the Experimental Section, the larger PPS stars contain a small fraction of dimers. The whole relaxation spectrum can be described by a combination of four relaxation processes (see Figure 8), which are starting at high frequencies: (1) the α-relaxation, (2) the chain backbone relaxation between entanglements, (3) the conformational relaxation due to arm retraction, and (4) the conformational relaxation of the central bar of the H-shaped dimers.

For the α-relaxation we have used a generalized exponential relaxation time distribution, which is equivalent to a stretched exponential relaxation in the time domain. We have described relaxation process (2) by a series of Rouse modes. These expressions were used earlier to fit $G'(\omega)$ and $G''(\omega)$ obtained for unentangled PPO stars (see for details ref 32). For relaxation process (3) we have used the expressions given by Milner and McLeish[25] for the relaxation of star polymers. We have taken into account that the cross bar of the H-shaped

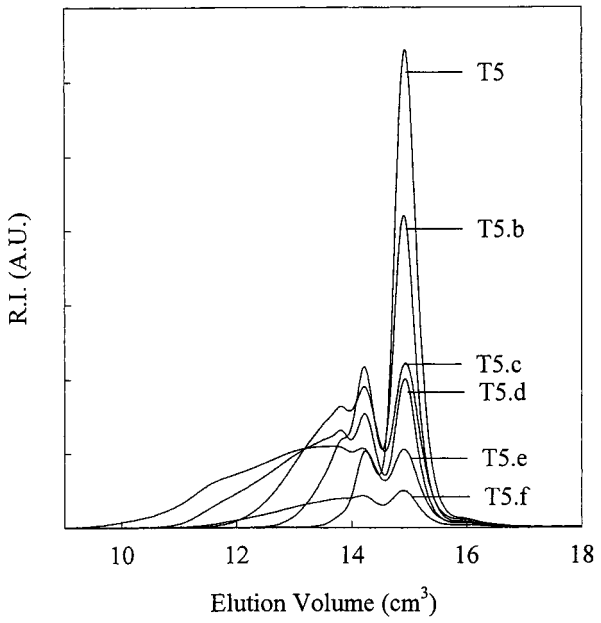

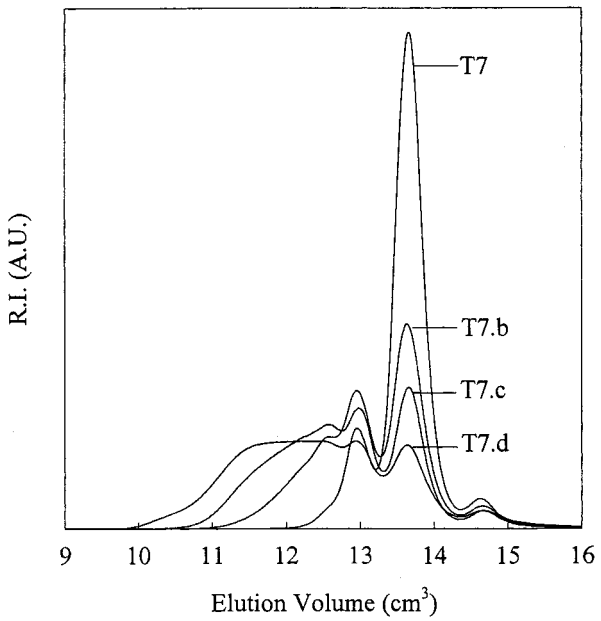

Figure 5. Chromatograms of end-linked PPS stars at different connectivity extents with $n_a = 72$ (top) and $n_a = (263)$ (bottom).

dimers does not contribute to the dynamic dilution during this relaxation process, although the effect is small. The best results were obtained using $M_e = 3.9$ kg/mol, which is close to the value estimated from the viscoelastic relaxation of linear PPS.[27] Relaxation (4) may again be described in terms of Rouse modes, because the concentration of the dimers is small so that

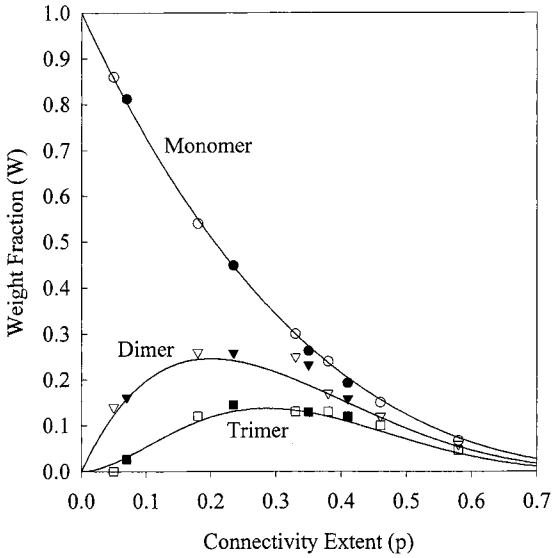

Figure 6. Comparison of the relative fraction of the first three oligomers with the prediction from mean field theory.

Table 2. Characteristics of End-Linked PPS Star Polymers

	r	M_w (kg/mol)[a]	M_w/M_n	*p*
T5.b	0.2	31.3	1.41	0.18
T5.c	0.4	56.7	2.10	0.33
T5.d	0.6	113.8	3.10	0.38
T5.e	0.8	265.4	6.29	0.46
T5.f	1	91.2[b]	3.11[b]	0.58
T7.b		146.4	1.84	0.24
T7.c		215.5	2.35	0.35
T7.d		378.5	3.75	0.41

[a] Using calibration with polystyrene standards. [b] Data for the sol fraction.

by the time the arms have relaxed they are effectively no longer entangled.

The data were fitted to a simple summation of these four contributions as is illustrated for the largest PPS star in Figure 8. The difficulty is to describe the transition between the different relaxation processes for which there is no theory. The best fit results were obtained by taking the fastest Rouse mode as about 10 times slower than the α-relaxation, by choosing the high-frequency cutoff of mode (3) at the slowest Rouse mode between entanglements (τ_e) and the high-frequency cutoff of mode (4) at the terminal relaxation time of the stars. However, the fits are not very sensitive to the choice of the transitions. The fit results are represented by the solid lines in Figure 7 and give a good description of the data for all samples. Of course, relaxation modes (3) and (4) do not occur for the smaller unentangled PPS stars.

The form of the α-relaxation is independent of the molar mass and is the same as reported earlier for linear PPS[27] (see Figure 9). Because of the limited dynamical range of the rheometer, the loss peak can only be measured over a small temperature range. The temperature dependence of the loss peak (ω_{max}) is independent of the molar mass if plotted as a function of $T - T_{gv}$. In this representation the effect of different glass transition temperatures is removed, and the temperature dependence is the same as for linear PPS.[26] We may conclude that the molar mass and the architecture influence the glass transition temperature, but not the frequency and temperature dependence of the α-relaxation. The same conclusion was drawn earlier from a comparison of linear and star PPO with a range of molar masses.[32]

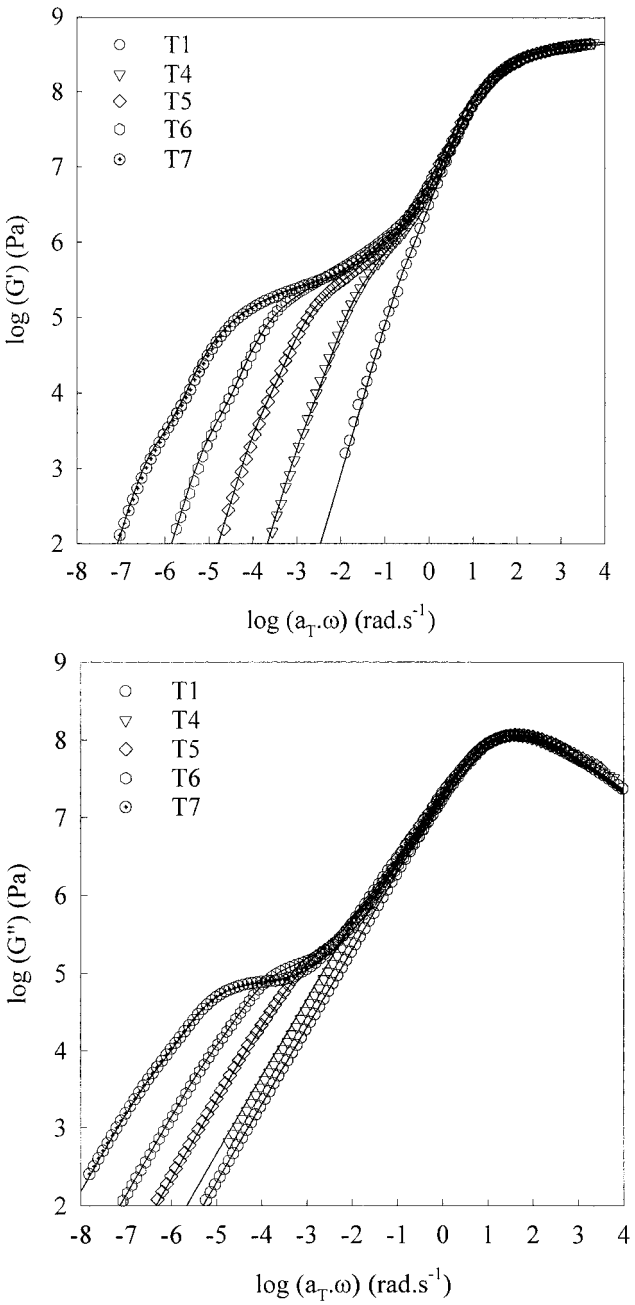

Figure 7. Master curves at $T_{ref} = T_{gv} + 5$ K of the storage (top) and loss (bottom) shear modulus for different PPS stars. The results for T2 and T3 were left out for clarity. The solid lines represent fit results; see text.

The terminal conformational relaxation time of the arms (mode (3)), τ_a, is plotted as a function of $T - T_{gv}$ for each sample in Figure 10. The solid lines represent fits to the VFT equation:

$$\log(\tau_a) = \log(\tau_0) + \frac{B}{T - T_0} \qquad (8)$$

The data could be fitted using the same values for $B = 525$ K and $T_0 = T_{gv} - 43$ K for each sample. The values of $\log(\tau_0)$ are summarized in Table 1. The same values for B and T_0 were also used to describe the results for linear PPS,[27] which shows that the molar mass and the architecture do not influence significantly the temper-

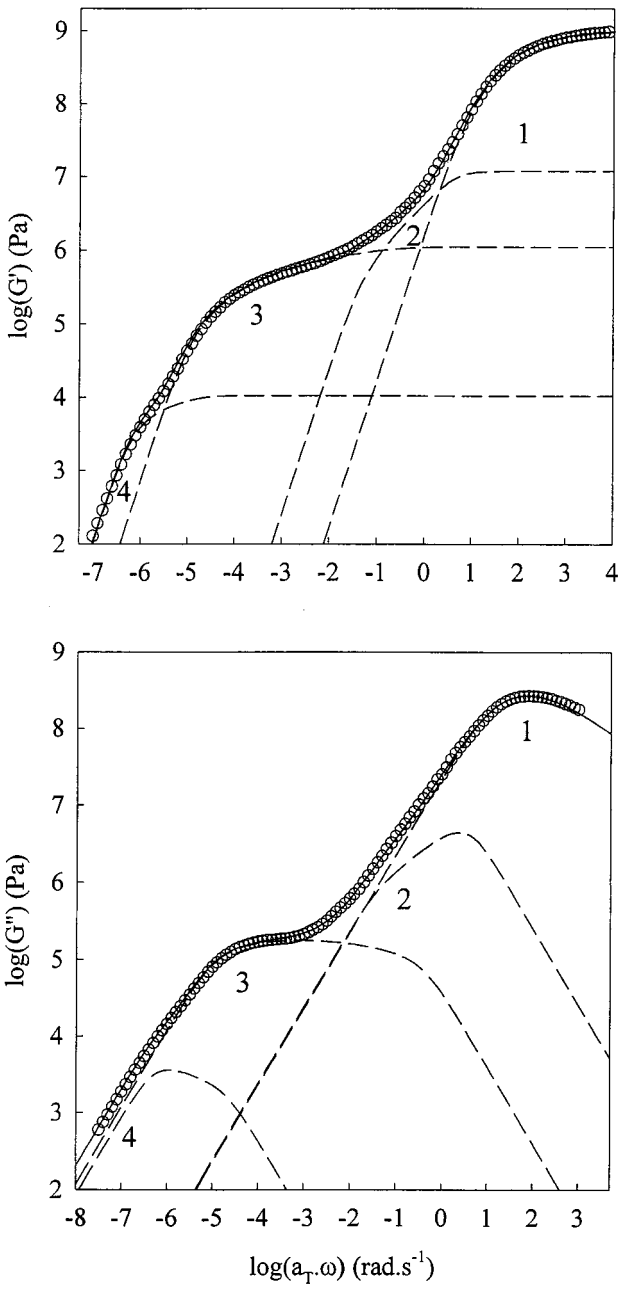

Figure 8. Decomposition of the four contributions to the relaxation of the storage (top) and loss (bottom) shear modulus for T7.

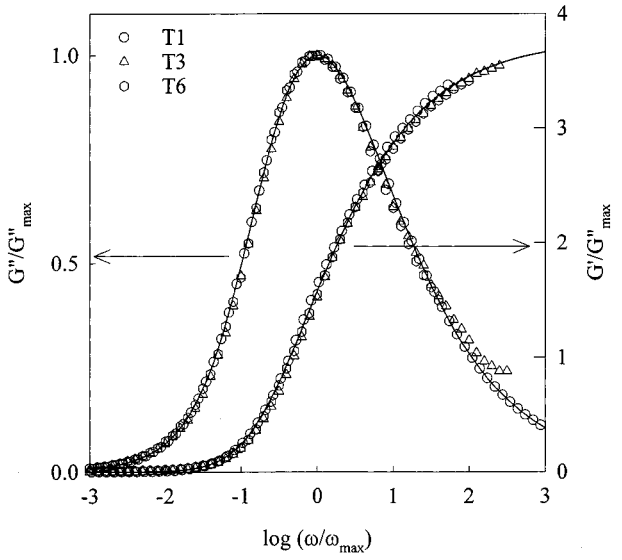

Figure 9. Semilogarithmic representation of the normalized storage and loss shear modulus for three samples. In this representation only the α-relaxation is clearly visible. The other samples showed the same behavior but were not included for clarity. The solid lines represent the results obtained for linear PPS.

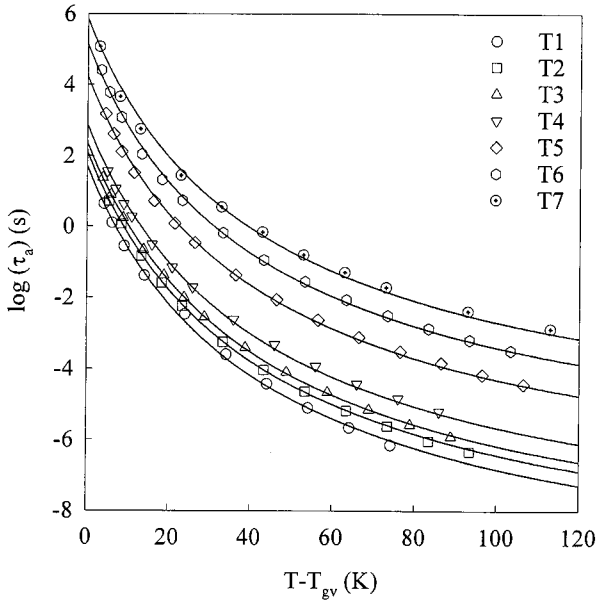

Figure 10. Reduced temperature dependence of the terminal relaxation time for the PPS stars with different molar masses. In this representation the effect of different glass transition temperature is removed.

ature dependence of the conformational relaxation, although they do influence the glass transition temperature.

In Figure 11 we have plotted τ_a at $T = T_{gv} + 100$ K as a function of number of segments per arm (n_a). For comparison, we have added the results obtained for linear PPS which may be viewed as a star with two arms. For the smaller samples that are not entangled ($n_a < n_e = 53$) τ_a is the relaxation time of the first Rouse mode which should be the same for linear and star PPS and increases with n_a as $\tau_a \propto n_a^2$. The solid line in Figure 11 has slope 2 and shows that the data have the expected behavior within the experimental error. For $n_a > n_e$ the data deviate upward. The dashed lines indicate the theoretical dependence for entangled stars[25] and linear chains ($\tau_a \approx \tau_e(n_a/n_e)^{3.4}$), respectively. The experimental results are compatible with the theoretical predictions, but the range of molar masses used in this study is not sufficient for a proper test of the theory. However, the viscoelastic relaxation of three-armed polyisoprene stars up to $n_a/n_e \approx 15$ was found to be in good agreement with the theory.[22]

The relaxation time of entangled arms increases very rapidly with n_a/n_e and is outside the experimental window for $n_a/n_e > 20$ even at 100 deg above the glass transition temperature. Not much is gained from measuring at higher temperatures because τ_a has a weak temperature dependence for $T > T_{gv} + 100$. In addition, PPS like most polymers degrades at high temperatures. We conclude that the analytical results obtained by Rubinstein et al. for the viscoelastic relaxation of highly entangled branched polymers cannot be tested experimentally.

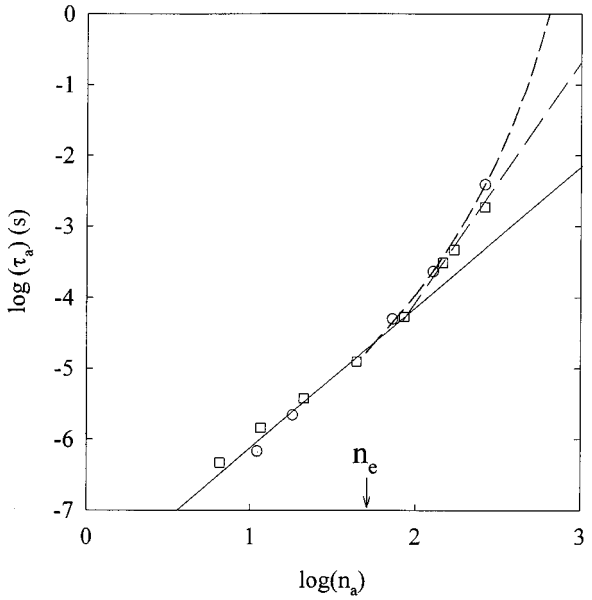

Figure 11. Dependence of the terminal relaxation time of linear (squares) and star (circles) PPS on the number of segments per arm. Linear PPS is considered as a star with two arms. The solid line shows the theoretical dependence for the relaxation of Rouse modes; the long dashed line, that of entangled linear chains and the short dashed line, that of entangled stars (see text).

Viscoelastic Relaxation of End-Linked Entangled Stars. In an earlier study unentangled PPO stars were end-linked using diisocyanate to form randomly branched polyurethane. PPS stars may be end-linked using the same linking agent leading to randomly branched poly(thiolcarbamate). However, for a controlled reaction the diisocyanate and the catalyst need to be thoroughly mixed with the PPS before the reaction advances significantly. This is not possible for large entangled PPS stars because they are extremely viscous. The largest PPS for which this method could be used was T5 with $n_a \approx n_e$. Samples with different fractions of end-linked T5 were prepared as described in the Experimental Section.

Figure 12 shows master curves of $G'(\omega)$ for end-linked T5 at different connectivity extents. The relaxation of free ends with $s = 1$ is clearly visible for all samples. At lower frequencies a second decay is observed which becomes slower and broader as the fraction and size of branched polymers increases. The master curves for the samples at $r = 0.8$ and 1.0 were constructed using only data obtained at $T < 40$ °C, because at higher temperatures $G'(\omega)$ no longer superimposes (see Figure 13). We observed the same effect for end-linked linear PPS,[30] and it is probably caused by physical association of thiolcarbamate groups. Unfortunately, the physical association means that we cannot study the slow conformational relaxation close to and beyond the gel point.

As described in the Experimental Section, we were able to end-link large entangled PPS stars (T7) by addition of various amounts of H_2O_2 to the reaction medium at the end of the polymerization. The disadvantage of this method is that the reaction cannot be done between the plates of the rheometer, which means that we can only investigate samples with low enough viscosity so that they can be manipulated. Figure 14 shows master curves of $G'(\omega)$ and $G''(\omega)$ at different fractions of end-linked star arms. Qualitatively, the results are the same as for end-linked T5, but the

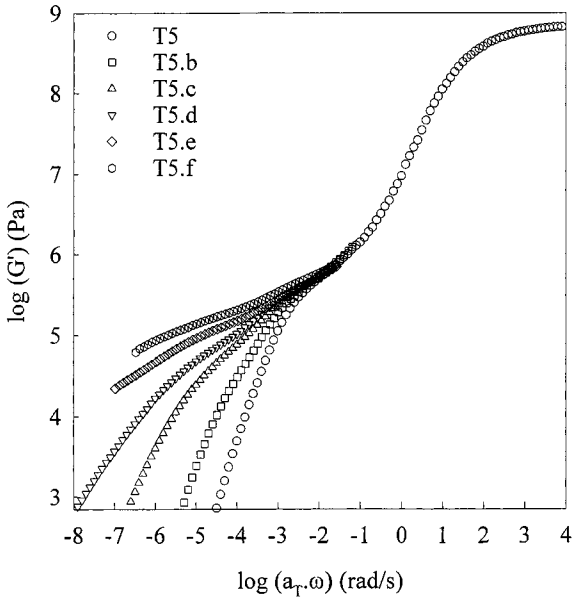

Figure 12. Master curves at $T_{ref} = T_{gv} + 5$ K of the storage shear modulus for end-linked PPS stars with $n_a = 72$ at different connectivity extents.

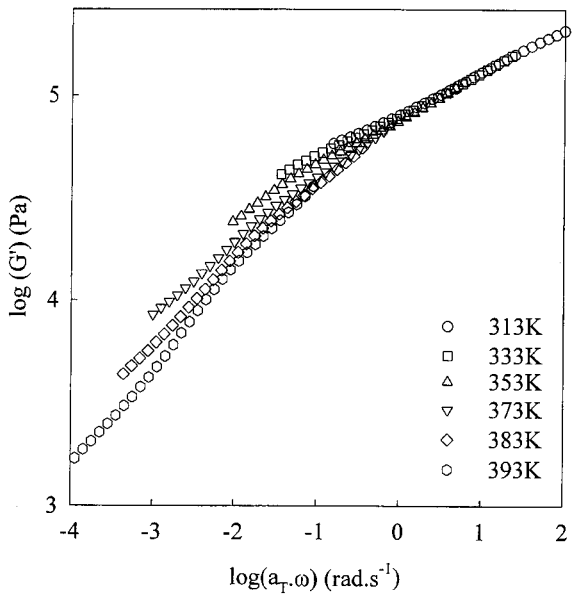

Figure 13. Master curve of the storage shear modulus for end-linked T5 with $r = 1.0$ (T5f) obtained at $T \geq 313$ K. $T_{ref} = 313$ K, and the data for $T > 313$ K were superimposed to those obtained at 313 K at high frequencies.

relaxation of the arms is shifted to lower frequencies. Again, one can clearly distinguish the relaxation of free-ends with $s = 1$ in the loss and storage spectra of end-linked T7. The amplitude of this relaxation decreases with increasing p, because the fraction of arms with $s > 1$ increases and is compatible with the value of $\phi(1)$ (see Figure 15). The decay shifts to lower frequencies with increasing p because arms with $s > 1$ have not yet relaxed at $\tau(1)$ so that the effect of dynamic dilution is reduced. The exponential prefactor ν in eq 1 varies from 15/24 if $\phi(1) = 1$, i.e., relaxation of stars in the melt, to 15/8 if $\phi(1) \rightarrow 0$, i.e., relaxation of dilute stars in a fixed network.[22]

The relaxation of arms with $s > 1$ leads to a second decay of the shear modulus which broadens with increasing p. The effect of dynamic dilution is very

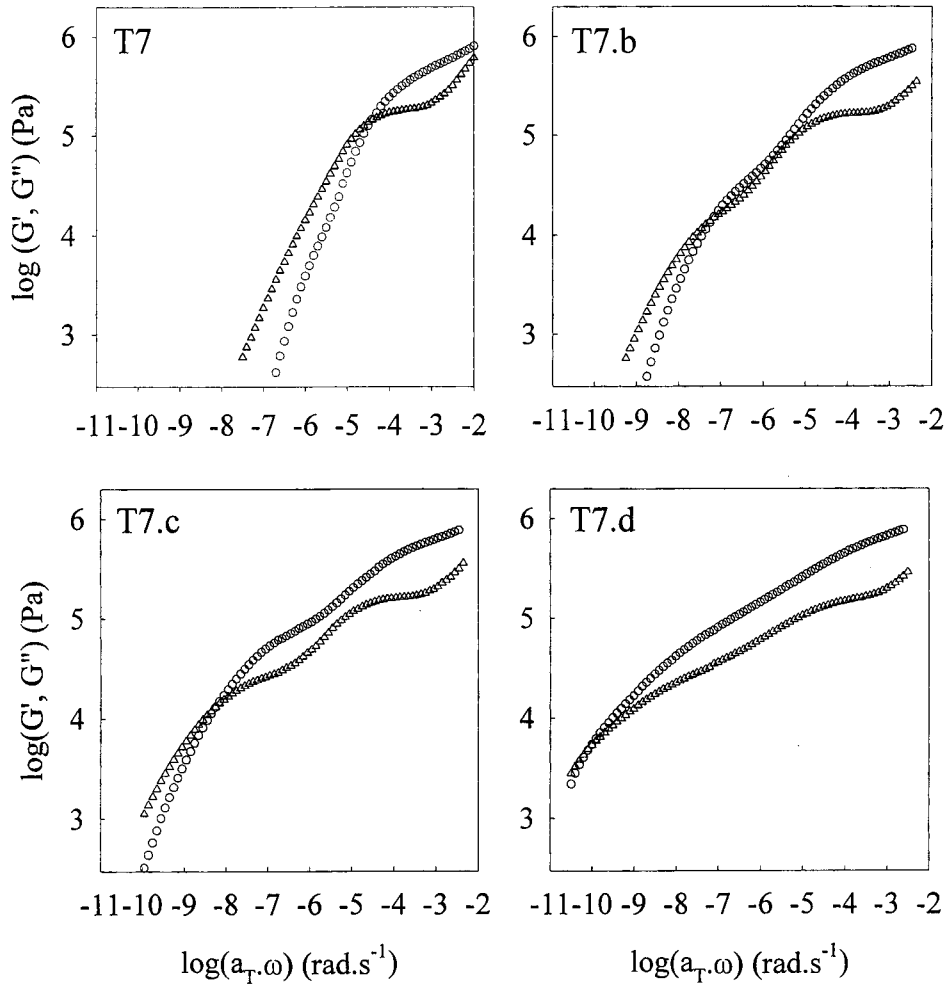

Figure 14. Master curves at $T_{ref} = T_{gv} + 5$ K of the storage (circles) and loss (triangles) shear modulus for end-linked PPS stars with $n_a = 263$ at different connectivity extents. For clarity, we only show the low-frequency relaxation. The high-frequency relaxation is independent of the connnectivity extent; see Figure 12.

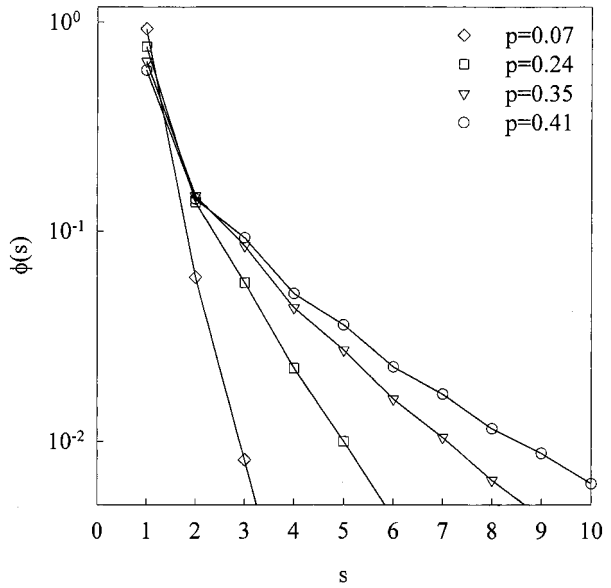

Figure 15. Fraction of star arms as a function of their seniority for s up to 10 at the connectivity extents of the end-linked T7 samples.

strong, and Figure 3 shows that arms with $s > 1$ are effectively unentangled if $p < 0.3$ for T7 for which $M/M_e \approx 5$. Arms with $s > 2$ are unentangled up to $p = 0.4$, and at the gel point arms with $s > 4$ are effectively unentangled. In all cases $M/M_e(s)$ is less than 2, which means that for the present system the effect of entanglements on the viscoelastic relaxation is only important for the free ends even at the gel point.

The viscoelastic decay of unentangled end-linked stars may be understood in terms of the relaxation of Rouse modes.[3,4] Both mean field theory and the percolation model predict that large branched polymers have a self-similar structure and that the number of polymers containing m stars $N(m)$ decreases with m according to a power law for $m > m_{min} \gg 1$. The self-similar structure and the power law size distribution lead to a power law frequency dependence of $G'(\omega)$ and $G''(\omega)$ at low frequencies. The viscoelastic relaxation of unentangled end-linked stars has been studied in detail for three-armed PPO stars with $n_a = 3$.[19] Very close to the gel point $G'(\omega)$ and $G''(\omega)$ showed indeed a power law decay, but only at frequencies more than 5 decades below the relaxation of the precursor stars. The broad crossover domain is due to relaxation of branched polymers with $m < m_{min}$.

The results were in quantitative agreement with the percolation model and not with mean field theory. The failure of mean field theory is to be expected, because it predicts that $M \propto R_g^4$, which implies that the density of the branched polymers increases with $m^{0.25}$. Consequently, for large m the density is no longer small so that loop formation and the effect of steric hindrance

are no longer negligible as is assumed in mean field theory. The density of the precursors decreases with increasing molar mass, which means that the value of m where mean field theory begins to fail increases with the molar mass of the precursors. However, for large precursors the terminal relaxation time is already very long for small values of m. Therefore, in practice only the crossover domain can be observed with large precursors. The frequency dependence of $G'(\omega)$ and $G''(\omega)$ in the crossover domain is weak, and over a small range of frequencies it can in some cases be interpreted as a power law decay with a small exponent. This is perhaps the origin of the small power law exponents that have been reported for systems based on large precursors.[9−18] Indeed, Lusignan et al.[18] showed that the experimentally observed power law exponent decreases with increasing number of entanglements between branch points. However, regardless of the degree of entanglement of the precursors, at the gel point clusters above a given size will be unentangled and have the structure and size distribution of percolating clusters. Therefore, the observed lower power law exponents for entangled systems at the gel point characterize a transition to the percolation value. As we have shown here, the final power law dependence, which is the same for all systems, cannot be observed experimentally even if the degree of entanglement is moderate.

If the precursors are strongly entangled, only the relaxation of arms close to the edges, i.e., with low seniority, can be observed experimentally. As mentioned above, explicit calculations exist for star- and H-shaped polymers, and the relaxation of blends of polymers with different sizes and architectures has also been investigated. In principle, these calculations could be extended to calculate the relaxation of arms with low seniority of end-linked stars using mean field predictions for the structure and the volume fraction of each branched polymer. We did not attempt to do this calculation because it is very cumbersome and not relevant for the systems investigated here.

Conclusions

The viscoelastic relaxation of PPS stars is characterized by three different relaxation processes: the α-relaxation, the conformational relaxation on length scales between entanglements which is well described by a series of Rouse modes, and the conformational relaxation on larger length scales due to chain retraction.

Because of dynamic dilution, highly branched polymers formed by randomly cross-linking are effectively unentangled even if the precursors are strongly entangled. The terminal frequency dependence is therefore expected to be the same as that of systems based on small precursors, which was found to agree with the percolation model. However, this frequency dependence cannot be observed experimentally if entangled precursors are used because the relaxation times involved are far too long. In practice, only the relaxation of segments close to the edges of the branched polymers is observed.

References and Notes

(1) Durand, D.; Delsanti, M.; Adam, M.; Luck, J. M. *Europhys. Lett.* **1987**, *3*, 297.
(2) Winter, H. H. *Prog. Colloid Polym. Sci.* **1987**, *75*, 104.
(3) Adolf, D. B.; Martin, J. E.; Wilcoxon, J. P. *Macromolecules* **1990**, *23*, 527.
(4) Martin, J. E.; Adolf, D. *Annu. Rev. Phys. Chem.* **1991**, *42*, 311.
(5) Rubinstein, M.; Colby, R. H.; Gillmor, J. R. In *Space-Time Organization in Macromolecular Fluids*; Tanaka, F., Doi, M., Ohta, T., Eds.; Springer-Verlag: Berlin, 1989.
(6) Lairez, D.; Adam, M.; Emery, J. R.; Durand, D. *Macromolecules* **1992**, *25*, 286.
(7) Matejka, L. *Polym. Bull.* **1991**, *26*, 109.
(8) Chambon, F.; Winter, H. H. *J. Rheol.* **1987**, *31*, 683.
(9) Scalan, J. C.; Winter, H. H. *Macromolecules* **1991**, *24*, 47.
(10) Lusignan, C. P.; Mourey, T. H.; Wilson, J. C.; Colby, R. H. *Phys. Rev. E* **1995**, *52*, 6271.
(11) Te Nijenhius, K.; Winter, H. H. *Macromolecules* **1989**, *22*, 411.
(12) Winter, H. H. *Polym. Eng. Sci.* **1987**, *27*, 1698.
(13) Winter, H. H. *Prog. Colloid Polym. Sci.* **1987**, *750*, 104.
(14) Holly, E. E.; Venktaraman, S. K.; Chambon, F.; Winter, H. H. *J. Non-Newtonian Fluid Mech.* **1988**, *27*, 17.
(15) Mours, M.; Winter, H. H. *Macromolecules* **1996**, *29*, 7221.
(16) Koike, A.; Nemoto, N.; Takahashi, M.; Osaki, K. *Polymer* **1994**, *35*, 3005.
(17) Kjoniksen, A. L.; Nystrom, B. *Macromolecules* **1996**, *29*, 5215.
(18) Lusignan, C. P.; Mourey, T. H.; Wilson, J. C.; Colby, R. H. *Phys. Rev. E* **1999**, *60*, 5657.
(19) Randrianantoandro, H.; Nicolai, T.; Prochazka, F.; Durand, D. *Macromolecules* **1997**, *30*, 5897.
(20) Ferry, J. D. *Viscoelastic Properties of Polymers*, 2nd ed.; Wiley: New York, 1970.
(21) Doi, M.; Edwards, S. F. *The Theory of Polymer Dynamics*; Clarendon Press: Oxford, 1990.
(22) McLeish, T. C. B.; Milner, S. T. *Adv. Polym. Sci.* **1999**, *143*, 195.
(23) Rubinstein, M.; Zurek, S.; McLeish, TCB.; Ball R. C. *J. Phys. (Paris)* **1990**, *51*, 757.
(24) Rubinstein, M.; Colby, R. H. *Macromolecules* **1990**, *23*, 2753.
(25) Milner, S. T.; McLeish, T. C. B. *Macromolecules* **1999**, *30*, 2159.
(26) Nicol, E.; Bonnans-Plaisance, C.; Dony Ph.; Levesque, G. *Macromol. Chem. Phys.*, in press.
(27) Nicol, E.; Nicolai, T.; Durand, D. *Macromolecules* **1999**, *32*, 5893.
(28) Prochazka, F.; Nicolai, T.; Durand, D. *Macromolecules* **2000**, *33*, 1703.
(29) Nicolai, T.; Prochazka, F.; Durand, D. *J. Rheol.* **1999**, *43*, 1511.
(30) Nicol, E.; Durand, D.; Nicolai, T. *Macromolecules* **2001**, *34*, 59.
(31) Plazek, D. J.; Schlosser, E.; Schönhals, A.; Ngai, K. L. *J. Chem. Phys.* **1993**, *98*, 6488.
(32) Nicolai, T.; Floudas, G. *Macromolecules* **1998**, *31*, 2578.
(33) Randrianantoandro, H.; Nicolai, T. *Macromolecules* **1997**, *30*, 2460.

MA002202L